JET Journal of Energy Technology

JET Volume 10 (2017) p.p. 11-27
Issue 4, December 2017
Type of article 1.01
www.fe.um.si/en/jet.html

A STRAIGHTFORWARD ANALYTICAL WAY OF EVALUATING THE SINGLE-PHASE INVERTER SPWM FREQUENCY SPECTRUM

ANALITIČEN POSTOPEK OCENITVE FREKVENČNEGA SPEKTRA SPWM IZHODNE NAPETOSTI ENOFAZNEGA RAZMERNIKA

Alenka Hren[1✉], Franc Mihalič[2]

Keywords: Fourier analysis, sinusoidal pulse-width modulation (SPWM), over-modulation phenomenon, single-phase inverter, total harmonic distortion (THD)

Abstract

For a DC-AC converter (inverter), a key element in renewable power supply systems, an output voltage of sinusoidal shape is required to assure a high-quality sustainable energy flow. Thus, through the modulation process, this property must be "incorporated" into the output voltage. This operation incurs some harmonic distortion into the inverter output voltage, which can have an undesired influence on the load. In the single- or three-phase systems (grid-connected, uninterrupted power supply systems (UPS) or motor drives), the high quality Total Harmonic Distortion (THD) factor must be considered; the voltage harmonic content also must be limited.

This paper provides a comprehensive spectrum analysis of a three-level output voltage in single-phase inverter. The output voltage is generated by triangular Sinusoidal Pulse-Width Modulation (SPWM) and, by using the Fourier analysis, Bessel functions and trigonometric equality, the high

[1✉] Corresponding author: dr. Alenka Hren, Tel.: +386 2 220 7332, Mailing address: University of Maribor, Faculty of Electrical Engineering and Computer Science, Koroška cesta 46, 2000 Maribor, E-mail address: alenka.hren@um.si

[2] dr. Franc Mihalič, University of Maribor, Faculty of Electrical Engineering and Computer Science, Koroška cesta 46, 2000 Maribor, E-mail address: franc.mihalic@um.si

harmonic components are extracted in a straightforward analytical way. Finally, the over-modulation phenomenon is also considered, and the procedure is experimentally validated.

Povzetek

Za zagotavljanje visokokakovostnega trajnostnega pretoka energije iz obnovljivih virov, mora razmerniško vezje, ki je ključni sestavni element pretvorniških sistemov, na izhodu zagotavljat sinusno obliko napetosti. To lastnost oz. obliko "vgradimo" v izhodno napetost razsmernika z izbranim modulacijskih postopkom, ki pa ob osnovni harmonski kompenenti vnaša v izhodno napetost tudi višje harmonske komponente. Te negativno vplivajo na breme razsmerniškega vezja in njegov izkoristek delovanja. V enofaznem ali trifaznem sistem (omrežne povezave, sistemi neprekinjenega napajanja ali motorni pogoni), mora razmerniško vezje delovati tudi z ustreznim, dovolj majhnim, faktorjem popačitve (Total Harmonic Distortion – THD), ki pa je odvisen prav od vsebnosti višjih harmonskih komponent v izhodni napetosti.

V članku je opisan postopek celovite analize harmonskega spektra trinivojske izhodne napetosti enofaznega razsmernika, pri čemer izhodno trinivojsko napetost generiramo s pomočjo sinusne trikotne modulacije (Sinusoidal Pulse-Width Modulation - SPWM). Z uporabo Fourierjeve analize, Besselovih funkcij in trigonometričnih enakosti lahko posamezne višje harmonske komponente izračunamo analitično. Opisan je tudi način delovanja razmernika in postopek izračuna harmonskih komponent v področju nadmodulacije. Pravilnost postopka analitičnega izračuna je eksperimentalno verificirana.

1 INTRODUCTION

The efficiency and stable operation of switching mode power inverters are of crucial importance for the sustainable production of the renewable energy sources connected to the utility grid, *[1]*, *[2]*, or that are a part of the standalone multifunctional power systems, *[3]*, and are both closely related to the used modulation strategy. The Pulse-Width Modulation (PWM) strategy has been in a focus of research for many decades, *[4]*, and remains an active research topic, *[5]*, *[6]*, due to its widespread usage in many fields of applications. Its usage is the most popular in the control of switching mode power converters for which it continues to represent a state-of-the-art solution.

Although, PWM has been used for many years and is well-described in many textbooks, *[7]–[10]*, the PWM algorithms for switching power converters have been the subject of intensive research, *[11]–[15]*, and some initiations of the analytical approach have been established, especially in *[11]*. Some PWM research work has been dedicated to the analytical way to understand the ac-ac converter modulation strategies, *[12]*, *[16]*, *[17]*. The necessity of the analysis of the PWM strategies in single-phase inverters began with the exploitation of the back-up systems (UPS) and with taking advantage of acoustics equipment in home appliances, *[18]–[23]*. Single-phase inverters in back-up systems are designed to adapt to the changing needs of load and input voltage sources, and the filter function can be solved by using passive filters, *[7]*. To minimize the filters' weight and size, it is also important to know the harmonic components of the inverter output voltage. Finally, it is generally accepted that the performance of an inverter that operates with arbitrary switching strategy is closely related to the frequency spectrum of its output voltage, *[11]*.

PWM can be implemented in many different forms. Pulse frequency is the most important parameter related to the PWM method and can be either constant or variable. A constant frequency PWM signal is obtained by comparing the modulation function with the carrier signal that can be in a sawtooth or a triangular shape. The most commonly used PWM form for a single-phase inverter is a naturally sampled PWM with a triangular (double-edge) carrier signal and a sinusoid as a modulation function, known as SPWM, since this kind of PWM improves the harmonic content of the pulse train considerably, *[24].*

In many textbooks, the authors only describe the "modern" approach for frequency spectrum evaluation based on Fast Fourier Transformation (FFT), probably due to the comfortability of this sophisticated mathematical tool. Understanding the PWM process using FFT was explored as a short-cut due to its spread appearance in many computer software tools, such as Matlab, LabVIEW SPICE, EWB, Simplorer, among others. These algorithms are also available in some electronic measuring instruments.

This paper presents a step-by-step analytical approach to the exact evaluation of single-phase inverter frequency spectrum obtained by naturally sampled SPWM. The proposed analytical way of evaluating SPWM frequency spectrum gives a comprehensive and deep insight into the mechanism of the harmonic components generation as well as a better foundation for understanding or even designing the SPWM devices in inverters. The main goal is to follow the SPWM procedure exactly by using the Fourier analysis, Bessel functions, and trigonometric equality in order to extract the high harmonic components in an analytical way. The switching (existing) function introduced by Wood, *[9]*, is used for a mathematical description of the modulation function. Additionally, the over-modulation phenomenon in a single-phase inverter and its analysis are considered and are presented in Section 3, where the obtained results were also experimentally verified in order to prove the procedure's correctness. Conclusions are summarized in Section 4.

2 SINGLE-PHASE FULL-BRIDGE INVERTER

When the high-efficiency, low-cost, and compact structure are of primary concern, the transformer-less inverter's topologies based on bridge configuration are the primary choice. Fig. 1 shows a single-phase full-bridge inverter circuit with a DC input voltage (v_{in}) and AC output voltage (v_{out}), the semiconductor switches' structure and the load structure. The inverter consists of two legs (half-bridges) with two semiconductor switches (IGBTs or MOSFETs and diode as indicated in Fig. 1), voltage sources indicated by (V_d/2) and current source (indicated by Load), representing the inverter output filter consisting of inductor *L*, capacitor *C*, and load resistance *R*.

The SPWM processes can generally be divided into two groups with respect to the inverter output voltage that can be either in two-level ($+V_d$ and $-V_d$) or three-level shape (with $+V_d$, 0 and $-V_d$). Since it is well known that the three-level output voltage has better spectrum properties, this kind of SPWM process will be considered in detail in this paper. Moreover, the first harmonic magnitude can be increased over V_d when over-modulation is applied, which means that the modulation index must exceed 1. With over-modulation, an increased magnitude of the first harmonic component is welcome in those situations in which the input voltage is decreased, but as a consequence of this phenomenon, *[10]*, additional spectrum lines appear, which also increases the Total Harmonic Distortion (THD) of the output signal.

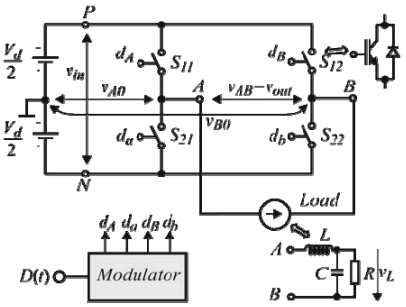

Figure 1: *Single-phase inverter structure; the semiconductor switch structure; the (current source) load structure.*

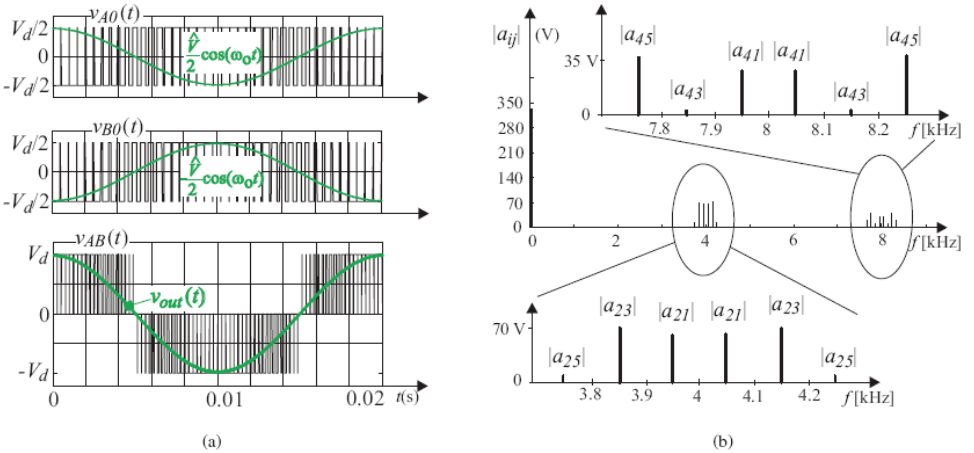

Figure 2: *(a) Output voltages: $v_{A0}(t)$, vB0(t) and $v_{AB}(t)$ with appropriate modulation functions and (b) Spectral lines for three-level output voltage.*

2.1 Generation of Three-Level Output Voltage

The whole inverter shown in Fig. 1 is divided into two half-bridge structures (legs). By using the first leg (switches S_{11} and S_{21}) the voltage $v_{A0}(t)$ ("first leg" voltage) and by using the second one (switches S_{12} and S_{22}) the voltage $v_{B0}(t)$ ("second leg" voltage) are generated at the inverter output, both with respect to the neutral point (shown in Fig. 1 and Fig. 2(a), respectively). If voltage $v_{A0}(t)$ precedes $v_{B0}(t)$ for an appropriate phase angle the inverter output voltage $v_{AB}(t)$ that equals the difference between voltages $v_{A0}(t)$ and $v_{B0}(t)$ will have the desired magnitude and desired three-level waveform, as indicated in Fig. 2(a). Voltages $v_{A0}(t)$ and $v_{B0}(t)$ are described as two switching events:

$$v_{A0}(t) = d_A(t)(V_d/2) + d_a(t)(-V_d/2), \tag{2.1}$$

$$v_{B0}(t) = d_B(t)(V_d/2) + d_b(t)(-V_d/2), \tag{2.2}$$

where the switching functions (see Fig. 3(a) and 3(b)) are:

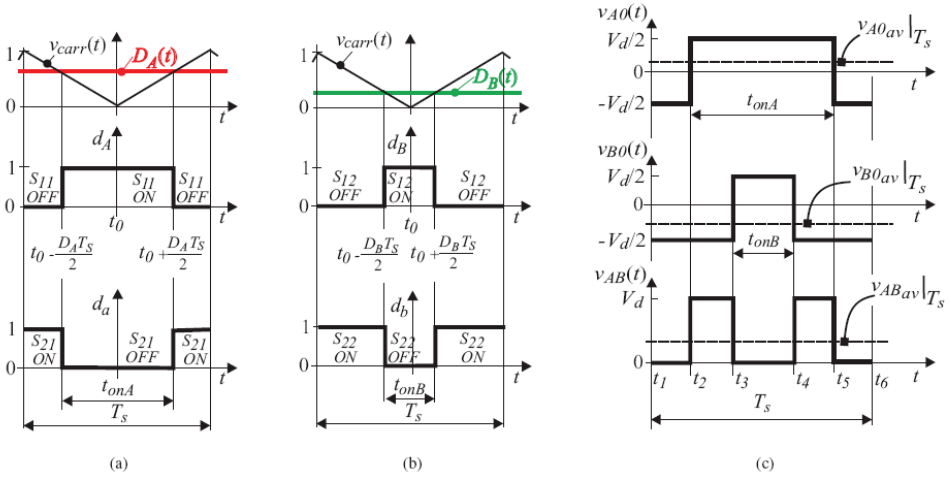

Figure 3: *Three-level switching functions generation (a,b) and, output voltages on the interval T_S (c): $v_{A0}(t)$, $v_{B0}(t)$ and $v_{AB}(t)$.*

$$d_A = \begin{cases} 1, & S_{11} = ON, \\ 0, & S_{11} = OFF, \end{cases} \quad d_a = \begin{cases} 1, & S_{21} = ON, \\ 0, & S_{21} = OFF, \end{cases} \tag{2.3}$$

$$d_B = \begin{cases} 1, & S_{12} = ON, \\ 0, & S_{12} = OFF, \end{cases} \quad d_b = \begin{cases} 1, & S_{22} = ON, \\ 0, & S_{22} = OFF. \end{cases} \tag{2.4}$$

In order to avoid the short circuit between the battery terminals P and N, the following conditions must be fulfilled:

$$d_A(t) + d_a(t) = 1, \tag{2.5}$$

$$d_B(t) + d_b(t) = 1. \tag{2.6}$$

Applying the above conditions in (2.1) and (2.2) follows to:

$$v_{A0}(t) = (2d_A(t) - 1)(V_d/2), \tag{2.7}$$

$$v_{B0}(t) = (2d_B(t) - 1)(V_d/2). \tag{2.8}$$

Referring to Fig. 3(c) (up and in the middle), the average value of the voltages vA0(t) and vB0(t) over the interval [0,Ts] can be evaluated as:

$$v_{A0_{av}}\Big|_{T_S} = \frac{1}{T_s}\int_{t1}^{t6} v_{A0}(t)dt = (2D_A(t) - 1)V_d/2, \tag{2.9}$$

$$v_{B0_{av}}\Big|_{T_S} = \frac{1}{T_s}\int_{t1}^{t6} v_{B0}(t)dt = (2D_B(t) - 1)V_d/2, \tag{2.10}$$

where $D_A(t)=t_{onA}/T_s$ and $D_B(t)=t_{onB}/T_s$ represent the corresponding duty cycle functions. If $T_s \ll T = 2\pi/\omega_o$ holds, the following approximation can be introduced:

$$v_{A0_{av}}(t)\Big|_{T_S} \cong v_{outA}(t), \tag{2.11}$$

$$v_{B0_{av}}(t)\Big|_{T_S} \cong v_{outB}(t). \tag{2.12}$$

Functions $v_{outA}(t)$ and $v_{outB}(t)$ represent the desired inverter output voltages for each half-bridge that can be expressed as:

$$v_{outA}(t) = +\frac{\hat{V}}{2}\cos(\omega_o t), \tag{2.13}$$

$$v_{outB}(t) = -\frac{\hat{V}}{2}\cos(\omega_o t). \tag{2.14}$$

Now, the duty cycle functions $D_A(t)$ and $D_B(t)$ can be evaluated from (2.9) to (2.14), respectively:

$$D_A(t) = \frac{1}{2} + \frac{1}{2}\frac{\hat{V}/2}{(V_d/2)}\cos(\omega_o t) = \frac{1}{2} + \frac{1}{2}m_I\cos(\omega_o t), \tag{2.15}$$

$$D_A(t) = \frac{1}{2} - \frac{1}{2}\frac{\hat{V}/2}{(V_d/2)}\cos(\omega_o t) = \frac{1}{2} - \frac{1}{2}m_I\cos(\omega_o t), \tag{2.16}$$

where $m_I = \hat{V}/V_d$ is modulation index.

An auxiliary triangular carrier signal $v_{carr}(t)$ needs to be introduced in order to transform the duty cycle functions $D_A(t)$ and $D_B(t)$ into a switching function $d_A(t)$ and $d_B(t)$. Fig. 3(a) and 3(b) show the triangular carrier signal, and both switching functions signal, respectively. The switching functions $d_A(t)$ and $d_B(t)$ were obtained by a comparison of duty cycle functions $D_A(t)$ and $D_B(t)$ with $v_{carr}(t)$ as follows:

$$d_A = \begin{cases} 1, & D_A(t) \geq v_{carr}(t), \\ 0, & D_A(t) < v_{carr}(t), \end{cases} \quad d_B = \begin{cases} 1, & D_B(t) \geq v_{carr}(t), \\ 0, & D_A(t) < v_{carr}(t). \end{cases} \tag{2.17}$$

The above-described procedure enables the generation of the triggering pulses in electrical circuits for all the semiconductor switches in the inverter. When referring to Fig. 4, the comparators (*comp*) compare the duty cycle functions $D_A(t)$ and $D_B(t)$ with triangular carrier signal (v_{carr}) and the signals $d_A(t)$, $d_a(t)$, $d_B(t)$ and $d_b(t)$ are obtained according to (2.5), (2.6) and (2.17).

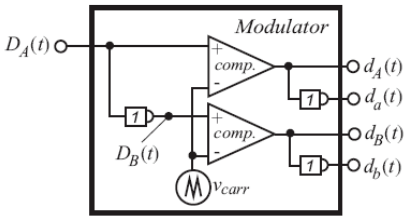

Figure 4: *Modulator block-scheme.*

The switching signals generated according to (2.17) can be considered to be periodic signals on the time interval $[0, T_s]$. When they are provided to the inverter switches, the three-level voltage (as shown in Fig. 2(a) and Fig. 3, respectively) appears at the inverter output:

$$v_{AB}(t)=\begin{cases}+V_d, & d_A(t)=1,\, d_B(t)=0,\, D_A(t)\geq D_B(t),\\ 0, & d_A(t)=0,\, d_B(t)=0 \vee d_A(t)=1, d_B(t)=1,\\ -V_d, & d_A(t)=0,\, d_B(t)=0, D_A(t)<D_B(t).\end{cases} \tag{2.18}$$

It is well known that any periodic signal of period T_s can be expanded into a trigonometric Fourier series form:

$$d_A(t)=\frac{a_0}{2}+\sum_{n=1}^{\infty}(a_n\cos(n\omega_T t)+b_n\sin(n\omega_T t)), \tag{2.19}$$

where ω_T is the frequency of the triangular carrier signal ($\omega_T = 2\pi/T_s$), and the coefficients a_0, a_n and b_n form a set of real numbers associated uniquely with the function $d_A(t)$:

$$\begin{aligned} a_0&=\frac{2}{T_s}\int_{t_0}^{t_0+T_S} d_A(t)dt,\\ a_n&=\frac{2}{T_s}\int_{t_0}^{t_0+T_S} d_A(t)\cos(n\omega_T t)dt,\\ b_n&=\frac{2}{T_s}\int_{t_0}^{t_0+T_S} d_A(t)\sin(n\omega_T t)dt. \end{aligned} \tag{2.20}$$

Each term $a_n \cos(n\omega_T t) + b_n \sin(n\omega_T t)$ defines one harmonic function that occurs at integer multiples of the triangular carrier signal frequency $n\omega_T$. According to the signal waveform of the pulse train shown in Fig. 3(a), the Fourier coefficients can now be evaluated as:

$$d_A(t)=\begin{cases}1, & t_0-\frac{D_A(t)T_S}{2}\leq t\leq t_0+\frac{D_A(t)T_S}{2},\\ 0, & elsewhere.\end{cases} \tag{2.21}$$

In order to simplify the coefficient's calculation, the initial time $t_0 = 0$ is chosen, so the coefficient a_0 is:

$$a_0=\frac{2}{T_s}\int_{-\frac{D_A(t)T_S}{2}}^{+\frac{D_A(t)T_S}{2}} 1dt=2D_A(t) \tag{2.22}$$

Coefficients a_n are also calculated from (2.20):

$$a_0=\frac{2}{T_s}\int_{-\frac{D_A(t)T_S}{2}}^{+\frac{D_A(t)T_S}{2}} 1\cos(n\omega_T t)dt=\frac{2}{\pi}\frac{\sin(n\pi D_A(t))}{n} \tag{2.23}$$

and all coefficient b_n are equal to 0. According to (2.19) the Fourier series of $d_A(t)$ is:

$$d_A(t) = D_A(t) + \frac{2}{\pi}\sum_{n=1}^{\infty}\frac{\sin(n\pi D_A(t))}{n} \tag{2.24}$$

and also for the switching function $d_B(t)$:

$$d_B(t) = D_B(t) + \frac{2}{\pi}\sum_{n=1}^{\infty}\frac{\sin(n\pi D_A(t))}{n} \tag{2.25}$$

2.2 The Output Voltage Spectrum Calculation

The output voltage $v_{AB}(t)$ can be constructed simply by subtracting outputs $v_{A0}(t)$ and $v_{B0}(t)$. In practice, when the load is connected between terminals *A* and *B*, the voltage difference $v_{AB}(t)$ appears on it. When (2.8) is subtracted from (2.7) it follows to:

$$v_{AB}(t) = (d_A(t) - d_B(t))D_d \tag{2.26}$$

The switching functions $d_A(t)$ and $d_B(t)$ can be expanded by the Fourier series in (2.24) and (2.25), respectively, and after applying (2.26) the inverter output voltage $v_{AB}(t)$ can be expressed by using the Bessel function as described in *[7], [8], [10]*:

$$\begin{aligned} v_{AB}(t) = m_I V_d \cos(\omega_o t) + \frac{4V_d}{\pi}\sum_{n=1}^{\infty}\frac{1}{n}\Big[\\ \cos(\frac{n\pi}{2})J_1(\alpha)\big[\cos((n\omega_T+\omega_o)t)+\cos((n\omega_T-\omega_o)t)\big] \\ -\cos(\frac{n\pi}{2})J_3(\alpha)\big[\cos((n\omega_T+3\omega_o)t)+\cos((n\omega_T-3\omega_o)t)\big] \\ \cos(\frac{n\pi}{2})J_5(\alpha)\big[\cos((n\omega_T+5\omega_o)t)+\cos((n\omega_T-5\omega_o)t)\big]\dots\ \Big] \end{aligned} \tag{2.27}$$

where $\alpha = nm_I\pi/2$. The structure of the spectral line's appearance is evident from (2.27). The SPWM signal $v_{AB}(t)$ has a fundamental component that appears at the frequency ω_o and, in addition to at the triangular carrier signal frequency $2n\omega_T$, also contains the sideband harmonics at frequencies $n\omega_T + k\omega_o$, $n = 1,2,3,\dots\infty$, $k = \pm1,\pm2,\pm3,\dots\infty$. Since the value of $\cos(n\pi/2)$ is zero for every odd *n*, the spectral lines only appear around even multiples of the carrier frequency $f_T = \omega_T/(2\pi)$, which is indicated in Tables 1 and 2, respectively. Fig. 2(b) shows the spectrum lines for the single-phase inverter's three-level output voltage for the V_d = 330 V and m_I = 1, line frequency f_o = 50 Hz and f_T = 2 kHz. From all the analyses above and the obtained results, the following conclusions can be made:

- The spectrum lines appear only for every even multiplier of f_T,
- The triangular carrier signal frequency f_T = 2 kHz is present in the half-bridge voltages ($v_{A0}(t)$ and $v_{B0}(t)$ not considered separately), but the synthesized inverter's output voltage $v_{AB}(t)$ switching frequency is doubled, so the first higher harmonic component appears next to the 4 kHz, and
- Filter components are needed at the inverter output to extract the first harmonic component at the fundamental frequency and reject the high switching frequency components of the output voltage $v_{AB(t)}$. The doubled switching frequency allows reduction of the size and weight of the filter components.

Table 1: *Spectral lines around the second multiplier of triangle carrier signal frequency $2f_T$.*

a_{21}	$\frac{4V_d}{\pi}\frac{1}{2}\cos(\frac{2\pi}{2})J_1(\frac{2\pi}{2}m_l)$	-63.4 V
a_{23}	$-\frac{4V_d}{\pi}\frac{1}{2}\cos(\frac{2\pi}{2})J_3(\frac{2\pi}{2}m_l)$	74.3 V
a_{25}	$-\frac{4V_d}{\pi}\frac{1}{2}\cos(\frac{2\pi}{2})J_5(\frac{2\pi}{2}m_l)$	-11.6 V

Table 2: *Spectral lines around the second multiplier of triangle carrier signal frequency $4f_T$.*

a_{41}	$\frac{4V_d}{\pi}\frac{1}{4}\cos(\frac{4\pi}{2})J_1(\frac{4\pi}{2}m_l)$	-23.7 V
a_{43}	$-\frac{4V_d}{\pi}\frac{1}{4}\cos(\frac{4\pi}{2})J_3(\frac{4\pi}{2}m_l)$	-3.2 V
a_{45}	$-\frac{4V_d}{\pi}\frac{1}{4}\cos(\frac{4\pi}{2})J_5(\frac{4\pi}{2}m_l)$	41.4 V

3 OVER-MODULATION PHENOMENON IN A SINGLE-PHASE INVERTER

The first harmonic magnitude for three-level output voltage (see (2.27)) is defined by $a_f = m_l V_d$ and has a position at the angular frequency ω_o (or frequency f_o). Obviously, the maximum magnitude of the first harmonic equals V_d due to the range of $m_l \in (0,1)$. The first harmonic magnitude can be increased over V_d when over-modulation is applied, which means that the modulation index must exceed $m_l \in (0,1)$. With over-modulation, an increased magnitude of the first harmonic component is welcome in some applications but, as a consequence of this phenomenon, the additional low-frequency spectrum lines appear.

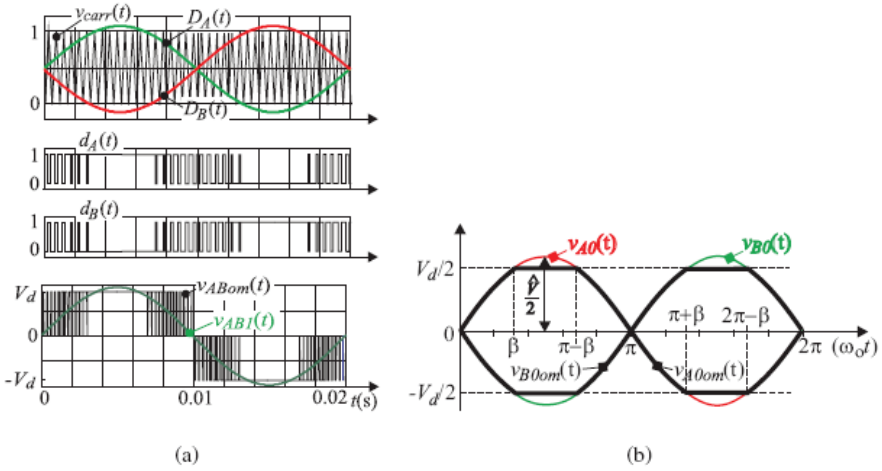

Figure 5: *Over-modulation procedure ($m_l = 1.2$): (a) Triangle carrier signal and duty cycle function $D_A(t)$, switching functions $d_A(t)$ and $d_B(t)$ waveforms. (b) Over-modulated desired half-bridge voltages $v_{A0om}(t)$ and $v_{B0om}(t)$.*

The three-level output voltage signal at the inverter output and over-modulation's influence on the frequency spectrum will be considered in the following subsections. Over-modulation appears when the duty cycle function $D_A(t)$ exceeds the magnitude of the high-frequency triangular carrier signal ($m_I > 1$). Fig. 5(a) shows a relationship between the triangular carrier signal and duty cycle function $D_A(t)$ and its influences on the switching functions $d_A(t)$ and $d_B(t)$ when a 20% over-modulation is applied, respectively.

3.1 The Duty Cycle Function Evaluation

Duty cycle functions can be evaluated in over-modulation as follows from (2.15) and (2.16) by applying $v_{A0om}(t)$ and $v_{B0om}(t)$ instead of $v_{A0}(t)$ exceeds $v_{B0}(t)$:

$$D_A(t) = \frac{t_A}{T_s} = \frac{1}{2} + \frac{1}{2}\frac{\hat{V}/2}{V_d/2} v_{A0om}(t) \tag{3.1}$$

$$D_B(t) = \frac{t_B}{T_s} = \frac{1}{2} + \frac{1}{2}\frac{\hat{V}/2}{V_d/2} v_{B0om}(t) \tag{3.2}$$

where of $v_{A0om}(t)$ and $v_{B0om}(t)$ are shown in Fig. 5(b) and are defined as follows:

$$v_{A0om}(t) = \begin{cases} \frac{\hat{V}}{2}\sin\omega_o t, & 0 \le \omega_o t < \beta, \\ +\frac{V_d}{2}, & \beta \le \omega_o t < (\pi - \beta), \\ \frac{\hat{V}}{2}\sin\omega_o t, & (\pi - \beta) \le \omega_o t < (\pi + \beta) \\ +\frac{V_d}{2}, & (\pi + \beta) \le \omega_o t < (2\pi - \beta) \\ \frac{\hat{V}}{2}\sin\omega_o t, & (2\pi - \beta) \le \omega_o t < 2\pi, \end{cases} \tag{3.3}$$

and

$$v_{B0om}(t) = \begin{cases} -\frac{\hat{V}}{2}\sin\omega_o t, & 0 \le \omega_o t < \beta, \\ -\frac{V_d}{2}, & \beta \le \omega_o t < (\pi - \beta), \\ -\frac{\hat{V}}{2}\sin\omega_o t, & (\pi - \beta) \le \omega_o t < (\pi + \beta) \\ +\frac{V_d}{2}, & (\pi + \beta) \le \omega_o t < (2\pi - \beta) \\ -\frac{\hat{V}}{2}\sin\omega_o t, & (2\pi - \beta) \le \omega_o t < 2\pi. \end{cases} \tag{3.4}$$

The voltages described by (3.3) and (3.4) can be expressed using Fourier series. The functions are odd, and due to this, the coefficients $a_n = 0$, so the voltages $v_{A0om}(t)$ and $v_{B0om}(t)$ are only

expressed by coefficients b_n, yielding:

$$v_{A0om}(t) = \sum_{k}^{\infty} b_k \sin(k\omega_o t), \tag{3.5}$$

$$v_{B0om}(t) = -\sum_{k}^{\infty} b_k \sin(k\omega_o t), \tag{3.6}$$

where k = 1,3,5,... and the Fourier coefficients b_k can be evaluated from (3.3) by taking the symmetry of the signal during the half of the period:

$$b_k = \frac{2}{T}\int_0^{T/2} \left[f(\omega_o t) - f(-\omega_o t)\right]\sin(k\omega_o t)dt, \tag{3.7}$$

where $T = 2\pi/\omega_o$, so it follows:

$$b_k = \frac{2V_d}{\pi}\left[\frac{m_I}{2}\left[\frac{\sin\left[(k-1)\beta\right]}{(k-1)} - \frac{\sin\left[(k+1)\beta\right]}{(k+1)}\right] + \frac{1}{k}\cos(k\beta)dt\right], \tag{3.8}$$

where β is computed as follows from Fig. 5(b):

$$\beta = \arcsin\left(\frac{V_d}{\hat{V}}\right) = \arcsin\left(\frac{1}{m_I}\right) \tag{3.9}$$

Substituting (3.5) and (3.6) into (3.1) and (3.2), respectively, the duty cycle functions become:

$$\begin{aligned} D_A(t) &= \frac{1}{2} + \frac{1}{V_d}\sum_{k}^{\infty} b_k \sin(k\omega_o t), \\ D_B(t) &= \frac{1}{2} - \frac{1}{V_d}\sum_{k}^{\infty} b_k \sin(k\omega_o t), \end{aligned} \tag{3.10}$$

3.2 The Over-Modulated Frequency Spectrum Calculation

The over-modulated output voltage can be evaluated from (2.26), (3.3) and (3.4):

$$v_{ABom}(t) = v_{A0om}(t) - v_{B0om}(t) = (d_A(t) - d_B(t))V_d \tag{3.11}$$

where the switching functions $d_A(t)$ and $d_B(t)$ can be evaluated by Fourier series as in (2.24) and (2.25), respectively and when combined with (3.10), the line to line voltage $v_{ABom}(t)$ can be expressed as:

$$v_{ABom}(t) = \underbrace{2\left(\sum_{k}^{\infty} b_k \cos(k\omega_o t)\right)}_{\text{LFSC}} + \text{HFSC}, \tag{3.12}$$

where LFSC means “Low-Frequency Spectral Components” and HFSC “High-Frequency Spectral Components”, which can be calculated as follows:

$$\text{HFSC} = \frac{4V_d}{\pi}\left(\sum_{n=1}^{\infty}\frac{1}{n}\cos\frac{n\pi}{2}\sin\left(\frac{n\pi}{V_d}\left(\sum_{k}^{\infty}b_k\cos(k\omega_o t)\right)\right)\sin n\omega_T t\right). \tag{3.13}$$

Eq. (3.12) consists of two parts: The first describes the low-frequency spectrum lines (next to the fundamental frequency ω_o), and the second describes the position and magnitudes of the high-frequency spectrum lines (next to the multipliers of triangle frequency ω_T). The over-modulation phenomenon is used in order to increase the first harmonic magnitude over the supply voltage when $\hat{V}_{AB1} \geq V_d$.

According to (3.8) and (3.12), the output voltage's low frequency harmonic components can be evaluated as follows:

$$\hat{V}_{ABk} = 2b_k = \frac{4V_d}{\pi}\left[\frac{m_l}{2}\left[\frac{\sin[(k-1)\beta]}{(k-1)} - \frac{\sin[(k+1)\beta]}{(k+1)}\right] + \frac{1}{k}\cos(k\beta)\right], \tag{3.14}$$

for the first, third, fifth and all odd spectral components, the (3.14) can be rewritten as (where in case of the first harmonic the division by zero can be avoided by replacing the function $\sin x = x$ for $m_l \gg$, or $\beta \ll$):

$$\hat{V}_{AB1} = \frac{4V_d}{\pi}\left[\frac{m_l}{2}\left[\beta - \frac{\sin(2\beta)}{2}\right] + \cos(\beta)\right], \tag{3.15}$$

$$\hat{V}_{AB3} = -\frac{4V_d}{\pi}\left[\frac{m_l}{2}\left[\frac{\sin(2\beta)}{2} - \frac{\sin(4\beta)}{4}\right] + \frac{1}{3}\cos(3\beta)\right], \tag{3.16}$$

$$\hat{V}_{AB5} = -\frac{4V_d}{\pi}\left[\frac{m_l}{2}\left[\frac{\sin(4\beta)}{4} - \frac{\sin(6\beta)}{6}\right] + \frac{1}{5}\cos(5\beta)\right]. \tag{3.16}$$

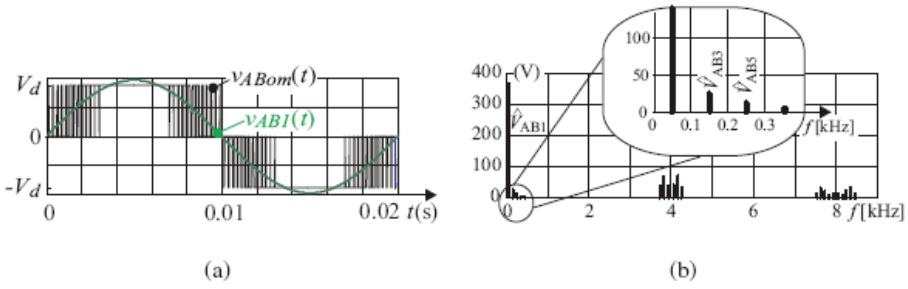

Figure 6: *(a) Over-modulated output voltage $v_{ABom}(t)$ and its first harmonic component $v_{AB1}(t)$. (b) The low and high harmonic components spectrum lines.*

Fig. 6(a) shows the three-level output voltage $v_{AB}(t)$ for V_d = 350 V, m_l = 1.2, line frequency f_o = 50 Hz and f_T = 2 kHz, while its spectrum lines are presented in Fig. 6. From all the analyses above and the obtained results for spectrum evaluation the following conclusions can be made:

- The HFSC spectrum lines calculated by (3.13) appear only for every even multiplier of f_T,

- The LFSC spectrum lines calculated by (3.12) are zoom-out in Fig. 6, while the calculated values for the magnitude as well as the normalized values V_{ABkn} for the first, third and fifth harmonic components are given in Table 3 for the case of 20% over-modulation. The magnitude of the first harmonic component $\hat{V}_{AB1}$ that exceeds the DC-voltage V_d by 10.4% was calculated by (3.15).

Table 3: *Spectral lines around the second multiplier of triangle carrier signal frequency $4f_T$.*

$\hat{V}_{AB1}$	$\frac{4V_d}{\pi}\left[\frac{m_I}{2}\left[\beta-\frac{\sin(2\beta)}{2}\right]+\cos(\beta)\right]$	386.6 V	V_{AB1n}	1.1046
$\hat{V}_{AB3}$	$-\frac{4V_d}{\pi}\left[\frac{m_I}{2}\left[\frac{\sin(2\beta)}{2}-\frac{\sin(4\beta)}{4}\right]+\frac{1}{3}\cos(3\beta)\right]$	-25.1 V	V_{AB3n}	0.0717
$\hat{V}_{AB5}$	$\frac{4V_d}{\pi}\left[\frac{m_I}{2}\left[\frac{\sin(4\beta)}{4}-\frac{\sin(6\beta)}{6}\right]+\frac{1}{5}\cos(5\beta)\right]$	-12.9 V	V_{AB5n}	0.0369

Fig. 7(a) shows the calculated first, second and third harmonic components versus modulation index changed from 0 to 2. When m_I exceeds 1, the magnitudes of harmonic components start to increase as follows from the presented over-modulation analysis.

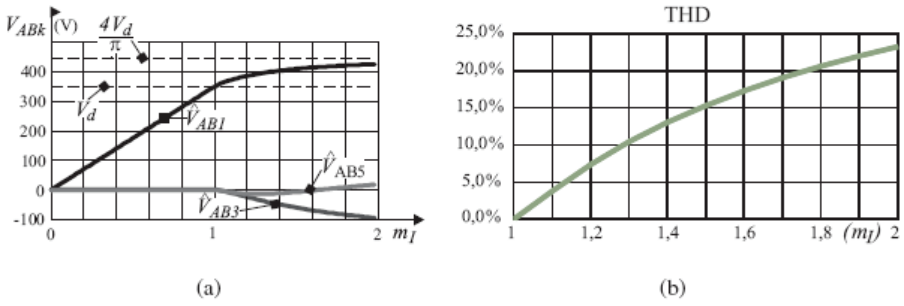

Figure 7: *(a) First, third and fifth harmonic components versus modulation index $m_I \in (0,2)$. (b) THD versus modulation index $m_I \in (1,2)$.*

To validate the presented procedure's correctness, a single-phase low-voltage (V_d = 20 V) inverter experimental set up based on the DRV8870DDAR integrated circuit was built in the laboratory. The described SPWM strategy was implemented using a Texas Instruments TMDSCNCD28335 control card that can be programmed in MATLAB SIMULINK and is ideal to use for initial evaluation and system prototyping. Output voltage over ohmic load was measured with a RIGOL DS2102A Digital storage oscilloscope. Fig. 8(a) presents the measured output voltage when the inverter operates in over-modulation with m_I = 1.2 while Fig. 8(b) shows its normalized frequency spectrum calculated by FFT in MATLAB. The obtained results show clearly that the normalized values for the first, third, and fifth harmonic components

match almost perfectly the predicted values calculated with the described procedure (see Table 3).

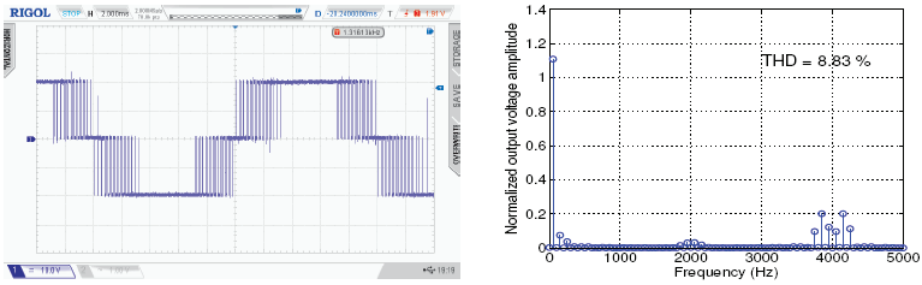

Figure 8: *(a) Inverter output voltage at m_I = 1.2 and (b) Its frequency spectrum.*

3.3 The Upper Limit Calculation

The upper limit is obtained when the modulation index m_I goes to infinity and, according to Fig. 5(b), the angle β goes to 0. The upper limit can be evaluated as follows:

$$\hat{V}_{ABk,\max} = \lim_{\beta\to\infty} \frac{4V_d}{\pi}\left[\frac{m_I}{2}\left[\frac{\sin[(k-1)\beta]}{(k-1)} - \frac{\sin[(k+1)\beta]}{(k+1)}\right] + \frac{1}{k}\cos(k\beta)\right] \tag{3.18}$$

and after calculation through a limit process:

$$\hat{V}_{ABk,\max} = \frac{4V_d}{\pi}\frac{1}{k} \tag{3.19}$$

It is evident from (3.19) that the upper limit for the first (fundamental, where k = 1) voltage harmonic component is:

$$\hat{V}_{ABk,\max} = \frac{4V_d}{\pi} \tag{3.20}$$

and is indicated as the upper limit line (i.e. at the square-wave output signal) in Fig. 7(a). The over-modulation operation of the inverter also has significant influence on the THD factor that is defined as:

$$THD = \frac{\sqrt{\sum_{k=2}^{n}\hat{V}_{ABk}^2}}{\hat{V}_{AB1}} \tag{3.21}$$

THD factor dependence on modulation index m_I is presented in Fig. 7(b). The maximum permissible THD factor is defined for different load types, so it is possible to set the necessary modulation index m_I which defines the first harmonic component magnitude $\hat{V}_{AB1}$ and, consequently from (3.15), the appropriate DC voltage V_d can be determined. In some special cases in which the available DC voltage supply V_d does not meet the requirements regarding the

magnitude of the output voltage $\hat{V}_{AB1}$ ($V_d < \hat{V}_{AB1} \leq \hat{V}_{AB1,\max}$), this over-modulation property allows us to omit the DC-DC boost converter in the power supply system.

4 CONCLUSION

In this paper, a straightforward, step-by-step SPWM frequency spectrum analysis has been presented for a single-phase inverter as an indispensable part of renewable energy source systems. The precise, analytical approach to SPWM signal analysis is rather unpopular among many engineers due to the relatively long and complicated procedure but, to understand these processes, it is necessary to take advantage of it. The additional reason that the analytical approach is not widely used in practice is due to the widespread usage of the MATLAB Software package. This program enables FFT numerical analysis of the PWM processes but, by using FFT, engineers do not gain an in-depth insight into the connections between the different quantities appearing in the formulas.

For three-level inverter output voltage, and over-modulation, principles of modulation algorithms have been developed here in a traditional analytical way. The electronic circuit of an SPWM modulator can be realized from the described algorithms by using new microcomputer technology and in the paper presented knowledge is also a good base for further investigation into SPWM switching strategies. The over-modulation phenomenon can help engineers to speculate using the inverter's parameters; for example, it can decrease the DC input voltage V_d and the output voltage will still have the necessary magnitude of the first harmonic component $\hat{V}_{AB1}$. The obtained results were experimentally verified in order to prove the procedure's correctness.

This analysis could be easily extended to three-phase inverters intended for electrical motor drive applications or grid-connected. And finally, the results of this analysis are also appropriate for further investigation of SPWM processes with respect to higher harmonic components' influence on losses for the different types of loads, as well as for filter design in the single-phase inverters used in UPS or grid-connected back-up systems.

References

[1] **G. Wang, G. Konstantinou, C.D. Townsend, J. Pou, S. Vazquez, G.D. Demetriades, and V.G. Agelidis:** *A review of power electronics for grid connection of utility-scale battery energy storage systems*, IEEE Trans. Sustainable Energy, vol. 27 no. 4, pp. 1778-1790, Oct. 2016

[2] **R. Theodorescu, M. Liserre, P. Rodríguez:** *Grid Converters for Photovoltaic and Wind Power Systems*, West Sussex: IEEE Press/John Wiley & Sons, Inc., 2011

[3] **F. Mihalič and A. Hren:** Isolated bi-directional DC-DC converter, *Journal of Energy Technology*, vol. 3, no. 3, pp. 27-40, Aug. 2010

[4] **H.S. Black:** *Modulation Theory*, New York: Van Nostrand Reinhold Company, 1953

[5] **M. Odavic, M. Summer, P. Zanchetta, and J.C. Clare:** *A theoretical analysis of the harmonic content of PWM waveforms for multiplefrequency modulators, IEEE Trans. Power Electronics*, vol. 25, no. 1, pp. 131-141, Jan. 2010

[6] **G. Fedele and D. Frascino:** *Spectral analysis of class of dc-ac PWM inverters by Kapteyn series,* IEEE Trans. Power Electronics, vol. 25, no. 4, pp. 839-849, April 2010

[7] **N. Mohan, T.M. Undeland, W.P. Robbins:** *Power Electronics, Devices, Converter, Application and Design*, second ed., New York: John Wiley & Sons., 1995

[8] **R.W. Ericson, D. Maksimovic:** *Fundamentals of Power Electronics*, Dordrecht: Kluwer Academic Publisher, 2001

[9] **P. Wood:** *Switching Power Converters*, New York: Van Nostrand Reinhold Company, 1981

[10] **D.G. Holmes, T.A. Lipo:** *Pulse Width Modulation for Power Converters: Principles and Practice*, New York: IEEE Press/John Wiley & Sons, Inc., 2003

[11] **H.S. Patel and R.H. Hoft:** *Generalized technique of harmonic elimination and voltage control in thyristor inverters: Part I - Harmonic elimination*, IEEE Trans. Industry Applications, vol. IA-9, no. 3, pp. 310-317, May/Jun. 1973

[12] **A. Alesina and M.G.B. Venturini:** *Solid-state power conversion: a Fourier analysis approach to generalised transformer synthesis*, IEEE Trans. Circuits Systems, vol. CAS-28, no. 11, pp. 319-330, April 1981

[13] **J. Holtz:** *Pulsewidth modulation - A survey*, IEEE Trans. Industrial Electronics, vol. 39, no. 5, pp. 410-420, Oct. 1992

[14] **V.G. Agelidis, A.I. Balouktsis, and C. Cossar:** *On attaining the multiple solutions of selective harmonic elimination PWM three-level waveforms through function minimization*, IEEE Trans. Industrial Electronics, vol. 55, no. 3, pp. 996-1004, Mar. 2008

[15] **S.A. Saleh, C.R. Molonay, and M. Azzizur Rahman:** *Analysis and development of wavelet modulation for three-phase voltage source inverters*, IEEE Trans. Ind. Electron., vol. 58, no. 8, pp. 3330-3348, Aug. 2011

[16] **A. Alesina and M.G.B. Venturini**: *Analysis and design of optimum-amplitude nine-switch direct ac-ac converter*, IEEE Trans. Power Electronics, vol. 4, no. 1, pp. 101-112, Jan. 1989

[17] **M. MilanoviČ and B. Dobaj:** *Unity input displacement factor correction principle for direct ac to ac matrix converters based on modulation strategy*, IEEE Trans. Circuits Systems I, vol. 4, no. 2, pp. 221-230, Feb. 2000

[18] **H. Koizumi, K. Kurokawa, and S. Mori**: *Analysis of class D inverter with irregular driving patterns*, IEEE Trans. Circuits Syst. I, vol. 53, no. 3, pp. 677-687, Mar. 2006

[19] **K.M. Cho, W.S. Oh, Y.T. Kim, and H.J. Kim:** *A new switching strategy for pulse width modulation (PWM) power converters*, IEEE Trans. Ind. Electron., vol. 54, no. 1, pp. 330-337, Feb. 2007

[20] **S.R. Bowes and D. Holliday:** *Optimal regular-sampled pwm inverter control techniques*, IEEE Trans. Ind. Electron., vol. 54, no. 3, pp. 1547-1559, Jun. 2007

[21] **Q. Li, P. Wolfs:** *A review of the single phase photovoltaic module integrated converter topologies with three different DC link configurations*, IEEE Trans. Power Electron., vol. 23, no. 3, pp. 1320-1332, May 2008

[22] **R.H. Green and J.T. Boys:** *Implementation of pulsewidth modulated inverter modulation strategies*, IEEE Trans. Ind, Appl., vol. IA-18, no. 2, pp. 138-145, Mar./Apr. 1983

[23] **R.O. Caceres and I. Barbi:** *A boost dc-ac converter: analysis, design, and experimentation*, IEEE Trans. Power Electron., vol. 14, no. 1, pp. 134-141, Jan. 1999

[24] **Z. Song and D.V. Sarwate:** *The frequency spectrum of pulse width modulated signals*, Signal Processing, vol. 83, no. 10, pp. 2227-2258, 2003

Nomenclature

(Symbols)	(Symbol meaning)
b_k	Fourier series coefficients
β	cross-section angle in the over-modulation
$d_A(t)$	switching function
$D_A(t)$	duty-cycle function
$J_i(\alpha)$	Bessel functions
m_I	modulation index
ω_T	triangular carrier signal frequency
ω_o	fundamental output voltage frequency
FFT	fast Fourier transformation
HFSC	high-frequency spectral components
LFSC	low-frequency spectral components
SPWM	sinusoidal pulse-width modulation
THD	total harmonic distortion
UPS	uninterruptible power supply